CHEMISTRY OF MATERIALS

ARTICLE

pubs.acs.org/cm

Surface-Tethered Zwitterionic Ultrathin Antifouling Coatings on Reverse Osmosis Membranes by Initiated Chemical Vapor Deposition

Rong Yang,[†] Jingjing Xu,[†] Gozde Ozaydin-Ince,[‡] Sze Yinn Wong,[†] and Karen K. Gleason*[,†]

[†]Department of Chemical Engineering, Massachusetts Institute of Technology, 77 Massachusetts Avenue, Cambridge, Massachusetts 02139, United States

[‡]Faculty of Engineering and Natural Sciences, Sabanci University, Orhanlı, Tuzla 34956, Istanbul, Turkey

Supporting Information

ABSTRACT: Poly[2-(dimethylamino)ethyl methacrylate-*co*-ethylene glycol dimethacrylate] (PDE) thin films were synthesized via initiated chemical vapor deposition (iCVD) and reacted with 1,3-propane sultone to obtain the zwitterionic structure. The cross-linker ethylene glycol dimethacrylate (EGDMA) was utilized to make the copolymer insoluble in water. The composition of the copolymer was tuned by varying the flow rates of precursors and calculated from Fourier transform infrared spectroscopy (FTIR) spectra. The zwitterionic coatings were covalently grafted on to reverse osmosis (RO) membranes, and surface characterizations were carried out. Scanning electron microscope (SEM) and atomic force microscope (AFM) revealed that the iCVD zwitterionic coatings were conformal and smooth over the RO membrane, and the coating thickness can be measured by using ellipsometry. Salt rejection was not impaired by the coating. Permeation tests were carried out under different feed pressures, film thicknesses, and film compositions, showing a 15% to 43% reduction in permeation. Cell adhesion tests were carried out using *Escherichia coli*, and the coated RO membranes showed superior antifouling performance compared with the bare RO membrane. This is the first time that the library of iCVD functional groups has been extended to charged zwitterionic moieties, and the zwitterionic coatings have been applied on delicate substrates, such as RO membranes.

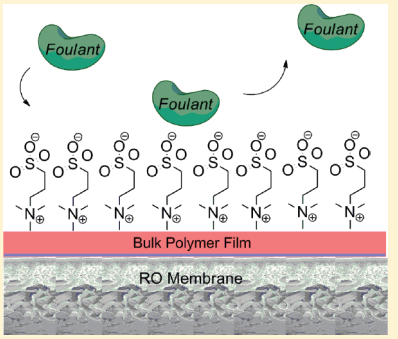

KEYWORDS: zwitterionic, chemical vapor deposition, reverse osmosis membrane, surface modification, bacterial adhesion, antifouling

INTRODUCTION

Biofouling is receiving increased attention in various applications, ranging from biomedical devices to water desalination membranes. Biofouling refers to the unintended accumulation of biopolymers or whole organisms (microorganisms, plants, algae, or animals) on wetted structures, and the subsequent formation of biofilms. It is always associated with the degraded performance or decreased efficiency of a system. For example, reverse osmosis (RO) membranes are one of the most popular water purifying materials because of their high salt rejection and permeation rates as well as their excellent chemical, thermal, and mechanical stability.[1] However, fouling of RO membranes can lead to reduction in flux, salt rejection impairment, and shortened membrane lifetime.[2] This limitation is considered the bottleneck to improve the efficiency of RO technology.[3] The biofouling process can be reduced or delayed by methods such as pretreating the feedwater,[4] periodic cleaning,[5] or surface modification of RO membranes.[3,6−10] However, the former two methods are costly and time-consuming, and periodic cleaning will shorten the membrane lifetime.[3] Surface modification such as physical adsorption and chemical bond formation are potential solutions to the biofouling problem.[6] However, the modification is no longer effective in preventing fouling once the deposition of foulants has taken place because the effect of solute/membrane interaction is reduced and replaced by solute/foulant interaction. Therefore, stable polymer architectures and surface modification strategies that impart ultralow-fouling characteristics to a surface are highly desired.

Poly(ethylene glycol) (PEG)/Oligo (ethylene glycol) (OEG) are the most widely used nonfouling materials.[11] PEG/OEG and other hydrophilic materials are less prone to biofouling because of hydration via hydrogen bonding.[12] However, their antifouling properties degrade during long-term applications. This failure has been attributed to oxidative degradation and enzymatic cleavage of PEG/OEG chains.[13] Zwitterionic-based materials can bind water molecules even more strongly than PEG/OEG chains via electrostatically induced hydration.[14−16] For this reason, zwitterionic-based materials are considered as the most promising candidates for preparation of ultralow fouling surfaces.[17,18] Zwitterionic-materials-modified surfaces can reduce the nonspecific protein adsorption to the ultralow level from single-protein solutions[19] and perform similarly or superiorly compared with PEG/OEG-modified surfaces in reducing

Received: November 1, 2010
Revised: January 20, 2011
Published: February 07, 2011

dx.doi.org/10.1021/cm1031392 | *Chem. Mater.* 2011, 23, 1263–1272

Table 1. Synthesis Methods of the Zwitterionic Coatings

method	SAMs[49, 50]	solution polymerization and solvent evaporation[15, 23]	ATRP[19, 22]	iCVD
conformality	high	low	high	high
nm- to um- scale thickness	×	×	×	√
no specific surface functionality required	×	√	×	√
solvent free	×	×	×	√
small post treatment roughness	√	×	√	√

plasma protein adsorption.[20,21] Furthermore, zwitterionic materials exhibit high resistance to bacterial adhesion and biofilm formation in long-term cell adhesion tests.[18,22]

Innovative techniques have been developed to synthesize zwitterionic coatings. Self-assembled monolayers (SAMs),[18] solution polymerization and solvent evaporation,[15,23] and atom transfer radical polymerization (ATRP)[19,21,24,25] are the most common (see Table 1). These methods generally involve harsh process conditions, for instance organic solvents, which may cause damage to delicate substrates (such as RO membrane). Louie et al. reported that after soaking the RO membrane in ethanol for 5 min, an eight- to ten- fold increase in Knudsen diffusion-based gas permeance was observed and this was attributed to an increase in the number or size of membrane defects generated by the ethanol treatment.[26] Therefore it can be inferred that organic solvents will cause damage to the delicate RO membrane. Methods such as SAMs and ATRP require specific surface functionality;[18−21,25] however, not all substrates possess or could possess (through pretreatment) the functional groups required. For example, SAMs only attach to gold surface;[21] specific initiators need to be grafted either by SAMs[19−21] or the pretreatment of 3,4-dihydroxyphenyl-L-alanine (DOPA)[18] prior to ATRP. DOPA has a cross-linked structure[27] and might decrease the permeation flux significantly if applied to membranes. In addition, solution polymerization and solvent evaporation may lead to high surface roughness, which is undesirable for the antifouling purpose. Poly[*N*,*N*-dimethyl-*N*-methacryloxyethyl-*N*-(3-sulfopropyl)] (PDMMSA or poly(sulfobetaine) or pSB) is one of the ultralow fouling zwitterionic polymers. Li and Jiang[18] attached pSB onto a gold surface coated with DOPA initiators, and the surface exhibited undetectable nonspecific protein adsorption (<0.3 ng cm^{-2}) from single-protein solutions by surface plasmon resonance (SPR)-sensor measurements. pSB coating can be synthesized through ATRP,[18] solution polymerization and solvent evaporation,[15,23] or incorporated into ultrafiltration membrane through water phase suspension polymerization and solution phase reaction.[9] While all those methods involve various organic solution treatments which might damage delicate substrates, using a vapor phase deposition method avoids the potential for this damage by solvents. However, the synthesis of zwitterionic polymers through vapor phase treatment has not yet been reported. Initiated chemical vapor deposition (iCVD) is an all-dry free-radical polymerization technique performed at low temperatures and low operating pressures,[28] which has shown great promise as a surface modification technique. It has been successfully utilized in synthesizing many distinct homopolymers,[29,30] random copolymers,[31,32] and alternating copolymers.[33] Poly(tetrafluoroethylene) has been coated on tissue paper using the iCVD technique.[34] The wetting behavior was changed without affecting the bulk properties of the substrate material. Nylon fabric has been coated with poly(dimethylamino)methyl styrene with grafting chemical vapor deposition (gCVD) which is a similar process to iCVD.[35] Because of the low substrate and filament temperatures and the solventless nature, iCVD enables the synthesis of low roughness films on virtually any substrate, even materials such as RO membranes which can be damaged by solvents or elevated temperatures.

Here, a copolymer containing pSB zwitterionic groups was synthesized through the iCVD technique and was applied onto an RO membrane for the first time. 2-(Dimethylamino)ethyl methacrylate (DMAEMA) was chosen as the precursor (vapor pressure = 0.45 Torr at 25 °C), which is compatible with the iCVD process. A random copolymer poly[2-(dimethylamino)-ethyl methacrylate-*co*-ethylene glycol dimethacrylate] (PDE) was synthesized and deposited as a thin film in a single step. Ethylene glycol dimethacrylate (EGDMA) was chosen as the cross-linker to increase the stability of the coating. The PDE copolymer was then reacted with the 1,3-propane sultone (PS) at the solid−gas interface to convert the DMAEMA group into a zwitterionic DMMSA functional group. (Figure 1) The zwitterionic structure was confirmed by FT-IR and XPS utilizing films deposited on silicon wafers. Coatings of identical composition were also grown directly on RO membranes. A strategy to covalently attach the polymer to RO membranes was developed to further increase the stability of the coating and adapt the coated membrane for long-term usage in water processing. Finally, surface properties of the coated RO membranes were characterized, along with their salt-rejection, permeation, and antifouling performance.

EXPERIMENTAL SECTION

Film Preparation and Derivatization. All iCVD films were deposited in a custom built vacuum reactor (Sharon Vacuum), as previously described.[29,36] Thermal excitations of the initiator were provided by heating a 0.5 mm Nickel/Chromium filament (80% Ni/20% Cr, Goodfellow) mounted in a parallel array, and the temperature was measured by a thermocouple attached to one of the filaments. The filament holder straddled the deposition stage which was maintained at a set point temperature using water cooling. The vertical distance between the filament and the stage was 2 cm.

All the chemicals were used as purchased without further purification. Silicon (Si) wafers (Wafer World, test grade) were coated with PDE copolymer without pretreatment. Prior to deposition, commercial RO membranes (Koch Membrane System, TFC-HR) were cleaned with filtered nitrogen, and then treated with maleic anhydride (MA, Fluka, puriss ≥99.0%). MA was heated to 65 °C in the glass jar, and the vapor was delivered into the vacuum chamber maintained at a pressure of 200 mTorr for 20 min. Filament temperature was kept at 200 °C to induce the MA to react with the secondary amide group in the RO barrier layer. At the end of the grafting reaction, flow of MA was stopped; the vacuum chamber was pumped out for a minimum of 1 h to remove any physisorbed MA from the surface of RO membranes.

During iCVD depositions, *tert*-butyl peroxide (TBPO, Aldrich, 97%) initiator and the nitrogen patch flow were fed to the reactor at room temperature through mass flow controllers (1479 MFC, MKS Instruments) at 1 and 0.5–3 sccm respectively. 2-(Dimethylamino)ethyl methacrylate (DMAEMA, Aldrich, 98%) and ethylene glycol dimethacrylate

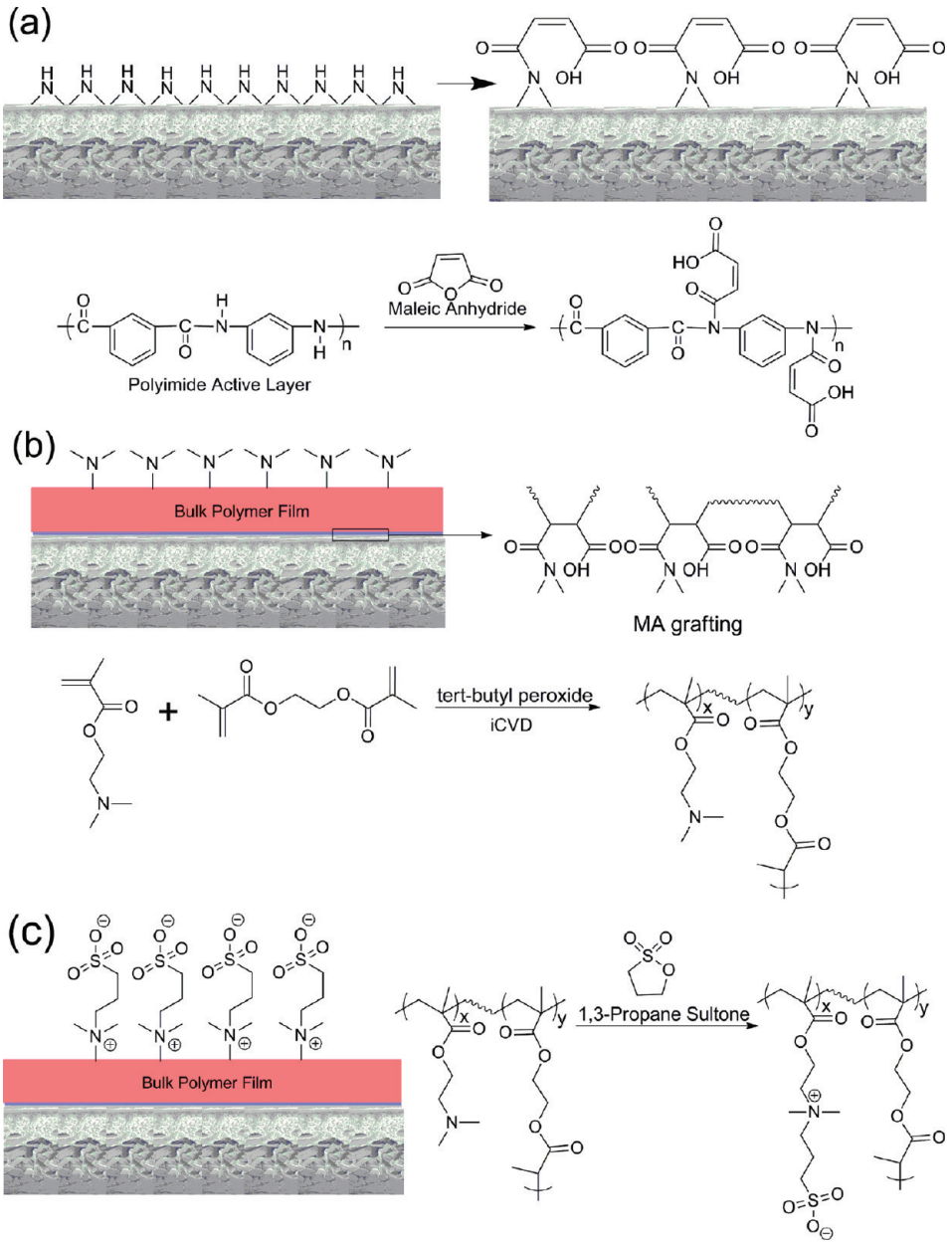

Figure 1. Surface modification process on RO membrane with zwitterionic films. (a) Treatment of RO membranes with MA for 20 min. (b) iCVD deposition of random copolymer poly[2-(dimethylamino)ethyl methacrylate-co-ethylene glycol dimethacrylate]. (c) Reaction with 1.3-propane sultone at 80 °C for 6 h.

(EGDMA, Aldrich, 98%) monomers were heated up to 55 and 80 °C in glass jars, respectively, and delivered into the reactor using needle valves. Systematic variation of the flow rate ratios was performed to yield high-zwitterionic-percentage, yet insoluble films of poly[2-(dimethylamino)ethyl methacrylate-co-ethylene glycol dimethacrylate] (PDE). Films were deposited at a filament temperature of 250 °C and a stage temperature of 20 °C. Total pressure in the vacuum chamber was maintained at 0.215 Torr for all depositions.

In situ interferometry with a 633 nm HeNe laser source (JDS Uniphase) was used to monitor the film growth and deposit desired thicknesses on Si substrates. A more accurate film thickness on the Si wafer substrates was measured post-deposition using a J.A. Woollam M-2000 spectroscopic ellipsometry at three different incidence angles (65°, 70°, 75°) using 190 wavelengths from 315 to 718 nm. The data were fit using a Cauchy−Urbach model.

After deposition, the PDE coated substrates were fixed in a crystallizing Dish (VWR) with 1 g of 1,3-propane sultone (Aldrich, 98%). The crystallizing dish was placed inside a vacuum oven (Shel Lab, 1415M) which was maintained at 60 Torr, 80 °C for 6 h to let 1,3-propane sultone vapor react with the coating on substrates.

Film Characterization. Fourier transform infrared (FTIR) measurements were performed on a Nicolet Nexus 870 ESP spectrometer in normal transmission mode. A deuterated triglycine sulfate (DTGS) KBr detector over the range of 400−4000 cm^{-1} was utilized with a 4 cm^{-1} resolution. Films on Si wafers were measured immediately after deposition or post-treatment, and measurements were averaged over 128 scans to improve the signal-to-noise ratio. All spectra were baseline corrected by subtracting a background spectrum of the Si wafer substrate and smoothed by averaging 17 adjacent points.

dx.doi.org/10.1021/cm1031392 |*Chem. Mater.* 2011, 23, 1263–1272

X-ray photoelectron spectroscopy (XPS) survey spectrum and high-resolution spectra of N_{1s} were obtained on a Kratos Axis Ultra spectrometer with a monochromatic Al Kα source. Samples were stored under vacuum overnight prior to analysis.

The thickness of the coating on the RO membrane was measured from scanning electron microscope (SEM) images. Membranes were frozen by liquid nitrogen and broken to obtain cross sections. Six nanometers of gold was sputter coated (Denton Desk II) onto the samples and SEM images were obtained by a JEOL JSM-6700F with acceleration voltage of 10 kV.

The surface roughness characterization of the coatings was performed using atomic force microscope (AFM, Veeco, Nanoscope V with Dimension 3100). Tapping mode was employed to prevent damage to the membrane surface morphology.

Hydrophilicity of coatings and bare RO membranes was evaluated by contact angle measurements performed on a goniometer equipped with an automatic dispenser (Model 500, Ramé-Hart) using a 2 μL DI water droplet.

Permeation Test. The permeation tests of the coated/bare membranes were performed using a commercial cross-flow membrane filtration unit (Sterlitech Corp., Sepa CF II) with a Hydracell Pump (M-03S) with DI water at 25 °C. The feed pressure was adjusted using a pressure control valve and a secondary metered valve. The flow rates of the feed were monitored by a vortex shedding flowmeter (FV101, Omega Engineering Inc.). The temperature of the feed was kept constant using a NESLAB chiller. The flow rates of the permeate were determined using a 100 mL metered flask. For the salt rejection calculations, a conductivity meter (CDH-152, Omega Engineering Inc.) was used.

Bacterial Adhesion Tests. *Escherichia coli* was used as the model microorganism. Static bacterial adhesion tests were performed following the protocol reported by Atar Adout and co-workers[8] with minor modifications. A single colony of *E. coli* was inoculated into Lysogeny broth (LB) medium and cultured overnight. The bacterial liquid was reinoculated into fresh LB medium and cultured until the logarithmic phase, centrifuged, and resuspended with fresh LB medium to the concentration of 4×10^7 cells/mL. The suspension was incubated with fluorescent dye fluorescein (Sigma-Aldrich) at 20 rpm and room temperature for 2 h. Then the bacterial liquid was centrifuged and resuspended with fresh LB medium to get rid of the excess fluorescein. Then membranes were placed into this dye-free suspension and incubated for 1 h. The membranes were then rinsed gently with a bacteria-free LB medium and observed under a fluorescent microscope (Carl Zeiss Axioskop 2 MAT).

RESULTS AND DISCUSSION

Film Synthesis and Characterization. The homopolymers pDMAEMA, pEGDMA, and copolymer PDE films were deposited by iCVD. The deposition rate and conformality of polymers were controlled by adjusting P^m/P^{sat}, the ratio of partial pressure of the monomer and its saturated partial pressure at the temperature of the substrate during deposition. This ratio is adjusted between 0.1 and 0.7 during the iCVD process to prevent condensation of the monomer inside the reactor. High P^m/P^{sat} values usually correspond to high deposition rate and poor conformality.[28] A P^{DMAEMA}/P^{sat} of ~0.4 and a P^{EGDMA}/P^{sat} of ~0.1 were adopted in the copolymer depositions after optimization.

Prior to deposition, the RO membranes were treated with maleic anhydride (Figure 1a, 1b); MA groups at the interface between the polymer film and substrate form covalent bonds with the substrate through the reaction between the anhydride and amide functional groups in RO membrane. Without MA grafting, zwitterionic films delaminated from the membrane surface when placed in water. The monomer DMAEMA was chosen because the tertiary amine group is the precursor of zwitterionic structure; the reaction between DMAEMA in polymer and 1,3-propane sultone in various organic solvents was previously reported.[9,15] However, homopolymer pDMAEMA was soluble in water; therefore ethylene glycol dimethacrylate (EGDMA) was used as the cross-linker to prevent the coating from dissolving in water. The copolymer shown in Figure 1b is a three-dimensional network; EGDMA groups link different polymer chains to one another. The chemical composition of copolymer was controlled by adjusting flow rates of precursors, as shown in Table 2. N_2 patch flow was used to keep the total flow rate constant, maintaining the same residence time for each deposition.

Table 2. Deposition Conditions for Five iCVD Coating Compositions

material	F(DMAEMA) (sccm)	F(EGDMA) (sccm)	F(TBPO) (sccm)	F(N_2) (sccm)	DMAEMA content in film[a] (%)
pDMAEMA	3.03	0	1	1	100
copolymer 1	3.27	0.16	1	0.5	70
copolymer 2	3.04	0.22	1	0.7	35
copolymer 3	1.79	0.18	1	2	15
pEGDMA	0	1.04	1	3	0

[a] DMAEMA Content in Film: calculated from the FTIR analysis.

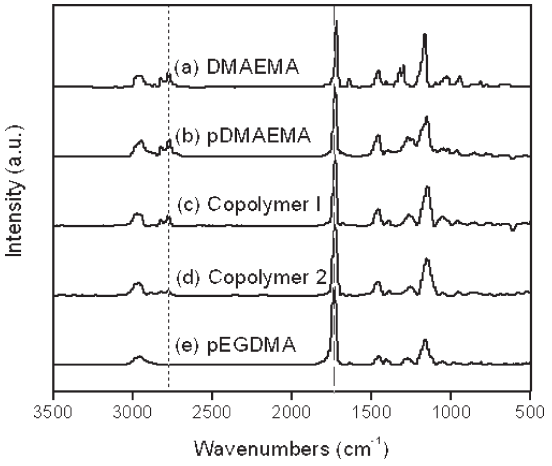

Figure 2. Fourier transform infrared spectroscopy (FTIR) spectra of (a) DMAEMA monomer, (b) iCVD deposited homopolymer of pDMAEMA, (c) copolymer with a pDMAEMA content of ~70%, (d) copolymer with a pDMAEMA content of ~35%, and (e) homopolymer of pEGDMA. The dotted line indicates the characteristic of tertiary amine group and the dashed line indicates the characteristic of the carbonyl in carboxylic acid groups.

The Fourier transform infrared spectroscopy (FTIR) spectra of DMAEMA monomer precursor, the as-deposited homopolymers pDMAEMA and pEGDMA, and copolymer films provide resolved features of the polymerized DMAEMA and EGDMA units. The vinyl bond in the monomer precursor contributes to the sharp C=C stretching mode at 1630 cm^{-1} (Figure 2a); the multiple peaks at 1299 and 1321 cm^{-1} are assigned to the conjugation structure between ester and vinyl bond[37] in the methacrylate precursor. The formation of polymer backbones

with saturated carbon groups is verified by the disappearance of those C═C characteristic peaks (Figure 2b to 2e). The double absorption at 2771 and 2822 cm^{-1} is characteristic of the tertiary amine structure in DMAEMA unit; this absorption is absent from quaternary amine spectra. The peak at 1721 cm^{-1}, which is characteristic of the carbonyl in carboxylic acid groups, was used along with the peak at 2771 cm^{-1} to calculate the content of DMAEMA unit in the copolymers (Figure 2c and 2d).

According to the Beer−Lambert equation,[37] the absorbance of a mode is proportional to the concentration of the moiety that is responsible for that particular mode, assuming that the bond oscillator strength is the same for each film. According to this equation, the areas under 2771 cm^{-1} and 1721 cm^{-1} are proportional to the concentration of tertiary amine and carbonyl groups respectively in the copolymers. Assuming these copolymers follow the Beer−Lambert equation, the chemical compositions can be calculated. In homopolymer pDMAEMA, the ratio of the carbonyl peak area to the amine peak area is 8.42 (denoted as r in eq 1). Using this ratio, the corresponding carbonyl intensity contributed by DMAEMA units can be obtained from the amine peak area, A_{amine}. Taking into account the two carbonyl bonds per EGDMA unit, the ratio of EGDMA units to DMAEMA units in a copolymer can be calculate as,

$$\frac{[\mathrm{EGDA}]}{[\mathrm{DMAEMA}]} = \frac{(A_{C=O} - r \cdot A_{amine})/2}{r \cdot A_{amine}} \qquad (1)$$

This method has previously been reported[38] for calculating the composition of p(2-hydroxyethyl methacrylate-*co*-ethylene glycol dimethacrylate). The calculated compositions (Table 2) were confirmed by XPS results (not shown here).

Reaction with 1,3-propane sultone was carried out following the synthesis of films. As shown in Figure 1c, the tertiary amine in DMAEMA was converted to a quaternary amine inner salt by reacting with 1,3-propane sultone vapor at 80 °C for 6 h. The FTIR spectrum (Figure 3a) confirms that the zwitterionic structure is obtained. The 1036 cm^{-1} adsorption is ascribed to the symmetric stretch vibration of the SO_3^- group,[37] and the characteristic peak of the tertiary amine (2771 cm^{-1}) is undetectable after the reaction, indicating the formation of a quaternary amine. However, this does not imply that the conversion to the zwitterionic structure in the bulk polymer is complete. The disappearance of the 2771 cm^{-1} peak after the reaction is largely due to the increased noise to signal ratio, as shown in the Supporting Information, Figure S1. This charged zwitterionic structure is also confirmed by the XPS nitrogen (1s) high resolution scan (Figure 3b and 3c). The peak around 398.8 eV corresponds to the quaternary amine (reaction product) in the sulfobetaine unit while the 396.5 eV peak is assigned to the tertiary amine in the DMAEMA unit (reactant). Before the reaction, the tertiary amine peak is dominant and the small amount of quaternary amine is attributed to the post-treatment adsorption of atmospheric CO_2,[39] which takes place in milliseconds and is inevitable. The occurrence of the reaction is indicated by the reduction of the tertiary peak and the increased intensity of the quaternary amine.

Both FTIR and XPS data confirmed the hypothesis that iCVD produced the zwitterionic copolymer poly[*N*,*N*-dimethyl-*N*-methacryloxyethyl-*N*-(3-sulfopropyl)-*co*-ethylene glycol dimethacrylate], which contains the sulfobetaine units.

Characterization of Surface Modification on RO Membrane. Commercial reverse osmosis (RO) membranes were coated with PDE (with 15% or 35% DMAEMA content in the PDE copolymer) and reacted with 1,3-propane sultone to form a zwitterionic copolymer layer on the RO barrier layer. The SEM images before and after the surface modification shown in Figure 4 confirm this. A high surface roughness was observed on the bare RO membrane cross-sectional SEM image. This was due to the mechanical stretching and tearing during the freeze fracture breaking of RO membrane, which has been reported by Ferlita and co-workers.[40] iCVD was controlled in situ with an interferometer monitoring the film thickness on the Si wafer,

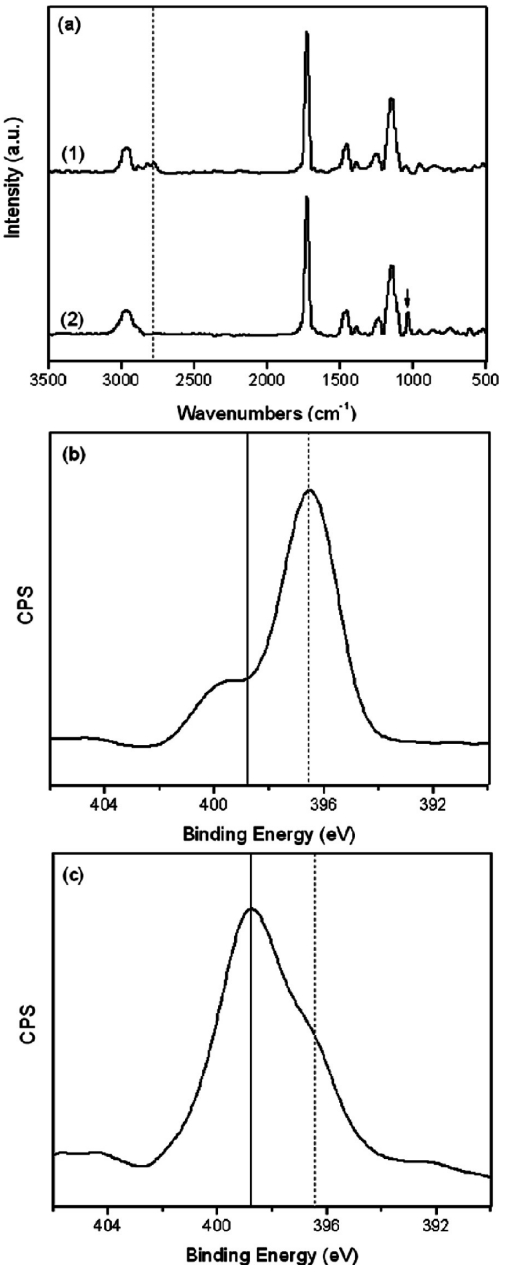

Figure 3. Confirmation of the formation of sulfobetaine unit: (a) the FT-IR spectra of copolymer 2 films (1) before reaction and (2) after reaction; the arrow indicates the characteristic peak of the SO_3^- group and the dashed line represents for the tertiary amine peak, which does not appear in the quaternary amine; (b) the XPS nitrogen high resolution scan before reaction and (c) after reaction with 1,3-propane sultone.

dx.doi.org/10.1021/cm1031392 |*Chem. Mater.* 2011, 23, 1263–1272

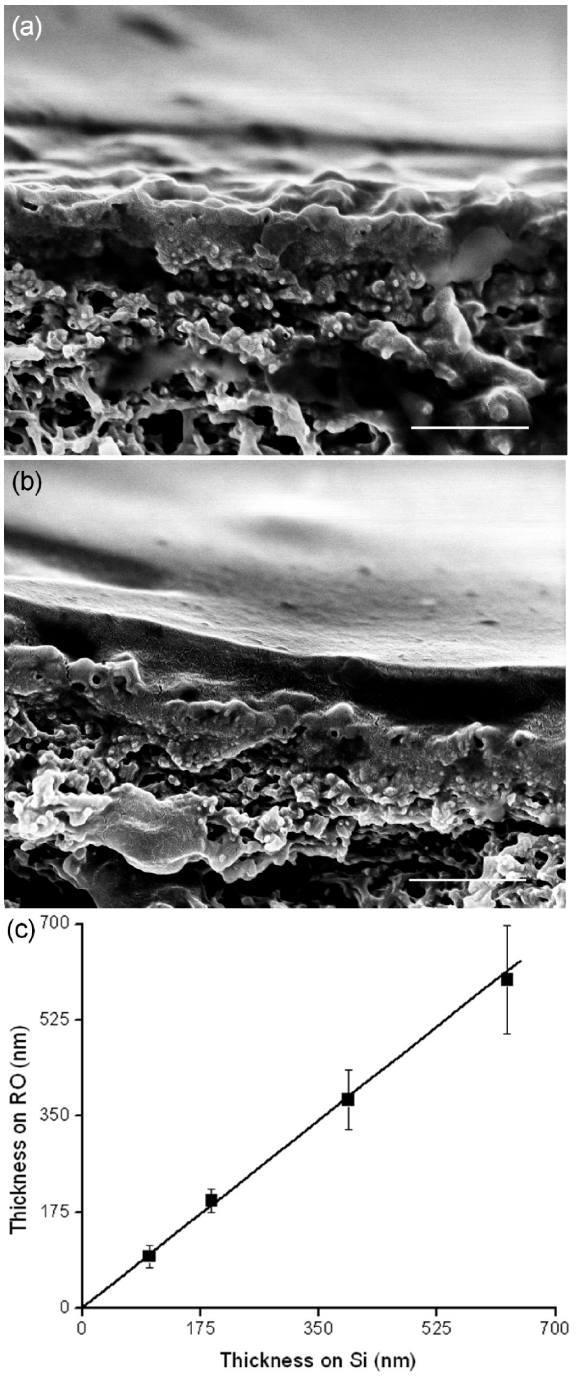

Figure 4. SEM images of cross sections of (a) the bare RO membrane and (b) after iCVD copolymer growth to 600 nm thickness (scale bar = 1 μm). For bare RO membrane, polysulfone layer and polyamide barrier layer (the non-porous top layer in (a)) were shown in the image. After iCVD deposition, it is very clear that a smooth and conformal coating formed on top of the polyamide. (c) The correlation between the film thickness on Si measured by ellipsometer and film thickness on the RO membrane measured by SEM images.

which was measured more precisely afterward with a variable angle spectroscopic ellipsometer. To check that the thickness of the coating on the Si wafer is representative of the thickness on the RO membrane, additional cross-sectional SEM measurements were performed on separate samples. Four PDE coatings (with the thickness of ~100, 200, 400, and 600 nm respectively)

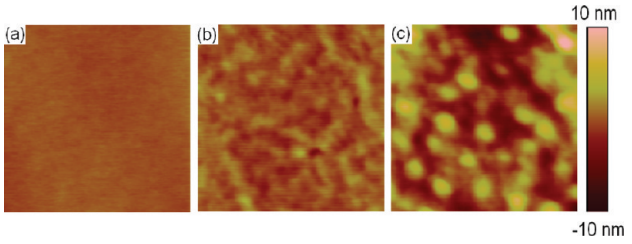

Figure 5. AFM images of (a) the bare RO membrane and after iCVD copolymer growth to (b) 30 nm and (c) 100 nm thickness. As the thickness increases the surface roughness increases. The rms roughness values for a, b, and c are 0.3, 0.9, and 2.8 nm, respectively.

were deposited on Si wafers and RO membranes by iCVD. For each coating, 10 SEM images were taken, and the average thickness was calculated. The relationship between the thicknesses on Si and the four SEM averages were plotted and shown in Figure 4c. There is a clear linear relation, and the slope of linear fitting is 0.97 (nm on RO/nm on Si) with an intercept of 1.91 (nm on RO). Therefore, the film thickness on Si is comparable to the film thickness on the RO membrane and will be used to estimate the film thickness on RO membrane.

In the permeation process of coated RO, water molecules have to diffuse through the coating layer in addition to the barrier layer; therefore, the coating thickness needs to be optimized for high water throughput and shear strength. The film thickness also affects the morphology of the RO membrane surface and consequently the antifouling property of the surface. A surface with micrometer scale roughness may induce an uneven flow distribution or channeling, thus acting as a physical barrier and entrapping bacteria.[41] The uneven flow distribution may also impair the throughput and lifetime of the membrane. Irregularities within tens of nanometers would provide a "shield" to attached proteins from shear forces by the disturbing static boundary layer. The probability of membrane fouling increases with the surface roughness also because rough surfaces have larger surface areas and more binding sites for foulants to attach. Furthermore, the formation of defects such as pinholes increases with surface roughness, which will accelerate the formation of the biofilm.

Because of the conformal nature of the iCVD process,[30,42,43] thin iCVD coatings have little effect on the surface roughness of RO membranes according to the AFM characterization of the iCVD coating on RO membranes. As shown in Figure 5, compared to the surface roughness of bare RO membranes (~0.3 ± 0.02 nm root-mean-square (rms) roughness), thin coatings (~30 nm) with 35% sulfobetaine increased the roughness to 0.9 ± 0.1 nm rms roughness, and thick coatings (~100 nm) with the same composition increases the surface roughness to 2.8 ± 0.2 nm rms roughness. The increase in roughness is due to the instability on the surface, which increases with the film thickness. However, the iCVD coated surface remains relatively smooth (<3 nm rms roughness). It is worth noting that at this low surface roughness, morphological effects on measured contact angles are minimal, and thus the contact angle data will primarily reflect the surface energy of the film. In addition, the 0.3 nm rms roughness refers to the roughness of the unsoaked bare RO membranes. It has been observed that after RO membranes are soaked in water, the surface roughness increases to 66.6 ± 4.1 nm (mean roughness), as shown in Supporting Information, Figure S2. Similar values have been reported by Xu et al. and Rahardianto et al. for the roughness of soaked RO membranes.[44,45]

Therefore, to minimize the surface roughness and maximize the throughput of coated membrane, thick coatings need to be prevented; therefore, a thickness of 30 nm was adopted as a compromise between the membrane performance and stability. The latter will be discussed in the next section.

Because of its effects on permeate throughput, hydrophilicity is another very important criterion for evaluating surface modification of membranes used in water processing. Static contact angles were analyzed to evaluate the surface hydrophilicity in this work. Measurements before and after the reaction with 1,3-propane sultone with the film on Si are 48.3 ± 1.0 degrees and 33.9 ± 0.9 degrees (for polymer 2, Table 3), respectively, which demonstrates the strong hydration via ionic solvation of zwitterionic units. For RO membranes, the contact angles before and after the modification are 41.9 ± 1.5 degrees and 33.3 ± 0.9 degrees (for polymer 2, Table 3), respectively. With decreased zwitterions and increased cross-linker content in the film (polymer 3), the contact angle becomes 60.7 ± 0.7 degrees. Therefore, it is clear that sulfobetaine units are the reason for increased hydrophilicity after modification.

Stability of Zwitterionic Thin Film. In commercial or industrial operations, RO membranes are used for prolonged periods to cut the cost. With proper pretreatment and cleaning, commercial RO membranes can last for up to 2 years.[46] To reduce fouling and protect the membrane, the antifouling coating has to be mechanically strong and adhesive to the RO membrane.

Table 3. Static Contact Angles of Coated/Bare RO Membranes Before/After Soaking

material	contact angle before soaking	contact angle after soaking
bare RO	41.9 ± 1.5	48.7 ± 1.3
copolymer 2	33.3 ± 0.9	40.5 ± 1.0
copolymer 3 grafted	60.7 ± 0.7	68.2 ± 0.6
copolymer 3 nongrafted	61.3 ± 1.0	49.4 ± 1.7

Covalent bonding of PDE to the RO membrane through MA grafting was required for stability in long-term usage. The grafting process is shown in Figure 1a. The anhydride moiety in MA reacted with the secondary amide group on the RO surface, and the MA vinyl bonds polymerized with DMAEMA and EGDMA to covalently bond the PDE coating to the substrate. To test the stability of the grafting method, iCVD coated membranes with and without MA treatment were put in DI water for 24 h. Contact angles before and after the soaking (Table 3) were used to indicate the condition of the iCVD coating. The coating composition of copolymer 3 was used because the difference between bare and coated membrane contact angles is largest for this composition. For the bare RO membrane and grafted iCVD coating, the contact angles increased by ~7 degrees after soaking, while for the non-grafted coating, the contact angle dropped to 49.4 ± 1.7 degrees, which is comparable to the bare RO membrane surface (48.7 ± 1.3). This drastic decrease in contact angle indicates the detachment of coating from the RO membrane during the soaking. As previously mentioned, soaked RO membranes have a higher surface roughness than unsoaked RO membranes; this increase in surface roughness explains the ~7 degrees of change of contact angles for bare RO membrane and grafted iCVD coating.

Permeation Tests. Permeation tests were performed with the bare RO membranes and RO membranes coated with different thicknesses and different compositions of iCVD coatings. The thickness of 30 nm and the composition of 35% sulfobetaine were adopted in the salt rejection tests.

Two pressures were used in the permeation tests to study the effect of hydrophilicity of the surface. Figure 6a and 6b are operated under 80 psi, while Figure 6c and 6d were operated under 300 psi. The permeation of water through an RO membrane consists of several steps. First, water molecules are adsorbed onto the membrane surface, and then these molecules will diffuse through the coating layer and barrier layer, and become permeate. The adsorption step is slower under low pressure than that under

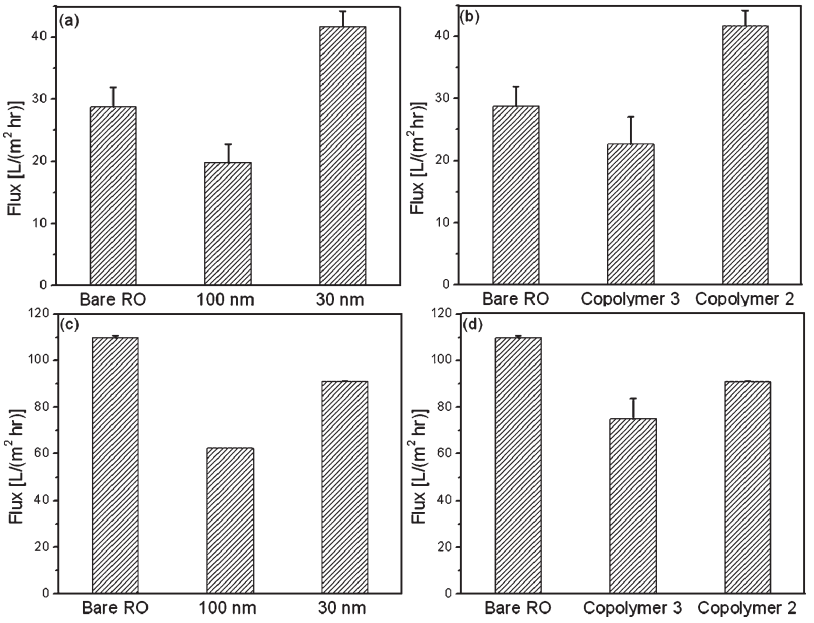

Figure 6. Permeation rates of DI water with pressure of 80 psi through bare RO membranes and the coated membranes of (a) different thicknesses with the pSB content of ~35%, (b) different compositions with the thickness of 30 nm and permeation rates with pressure of 300 psi of (c) different thicknesses with ~35% pSB content, and (d) different compositions with the thickness of 30 nm.

dx.doi.org/10.1021/cm1031392 |*Chem. Mater.* 2011, 23, 1263–1272

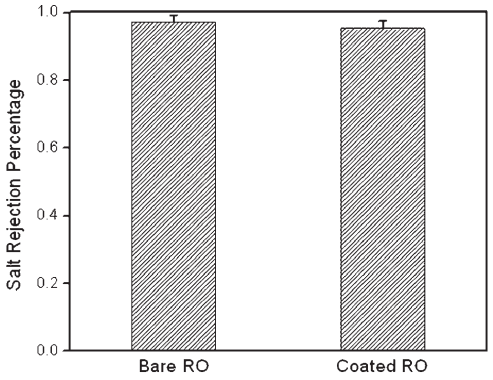

Figure 7. Salt rejection percentages of the bare and coated RO membranes. The coating chemistry has no effect on the salt rejection of the membranes.

high pressure; therefore the hydrophilicity of the surface plays a more important role in determining the permeation rate under low pressure. In Figure 6a, the composition of coating is 35% pSB. When the thickness was 30 nm, the permeation rate of the coated RO membranes became higher than the bare membrane because of the more hydrophilic surface after surface modification. However, with the film thickness of 100 nm, the diffusion through membrane became rate-limiting, and therefore the thicker coating induced slower permeation rate than bare RO membrane. Furthermore, when the composition of 15% sulfobetaine was adopted, a lower permeation flux was observed (Figure 6b). The surface hydrophilicity of the 15% pSB coating was less than bare RO, and the cross-link density in the bulk coating was higher than the 35% pSB coating, both of which contributed to the decreased permeation.

Under high pressure (300 psi), the diffusion step becomes the slow step; therefore coated membranes have lower permeation flux compared to bare RO membranes. With the increase of film thickness from 30 to 100 nm, the flux was further reduced from 91.1 L/h/m^2 to 62.3 L/h/m^2 compared to the 109.8 L/h/m^2 of bare RO membranes (Figure 6c). The flux can be increased by further decreasing the coating thickness. Increasing the surface hydrophilicity can also increase the permeation of coated membrane. The flux increased from 75.0 L/h/m^2 to 91.1 L/h/m^2 when the chemical composition of the coating was changed from 15% sulfobetaine to 35% sulfobetaine.

The salt rejection of the bare and coated membranes were measured by monitoring the conductivity of the permeate using a conductivity meter. The measurements were recorded every 2 min for 4 h. A 2000 ppm NaCl solution was used as the feed, and the tests were operated under 300 psi. The overall salt rejection of the bare RO membrane is around 97%. Figure 7 shows the salt rejection percentages for bare and coated membranes at the end of 4 h. The minor decrease in salt rejection (~2%) after coating is within the experiment error.

Cell Adhesion Tests. The antifouling capability of the zwitterionic surface modification was tested with *E. coli*. The attachment and settlement of bacteria is the key step in the formation of biofilm, and *E. coli* is a gram negative bacterium which is widely used in membrane antifouling studies.[8,47,48] In this work, the static adhesion of *E. coli* cells onto the zwitterionic films was studied and compared with bare RO membrane.

The membrane coupons (bare RO membranes and RO membranes coated with 30 nm zwitterionic films) were incubated with concentrated *E. coli* bacteria culture for 1 h, and then

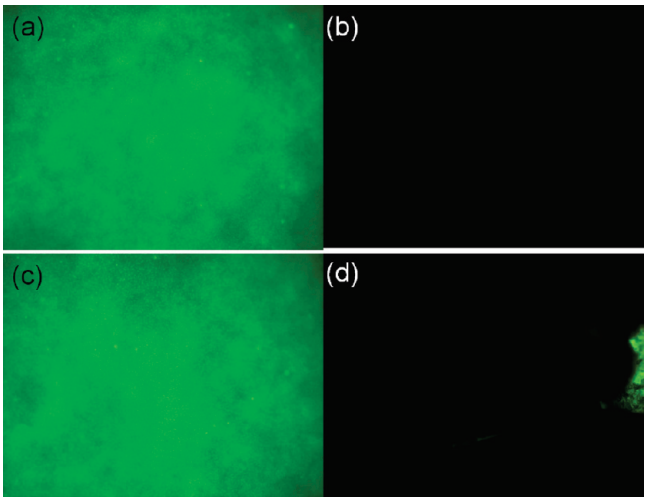

Figure 8. Fluorescence micrographs of (a) bare RO membrane, (b) RO membrane with 30 nm iCVD coating, (c) bare RO membrane, and (d) coated RO membrane (30 nm coating) with scratch, exhibiting the contrast between the antifouling capabilities of coated/uncoated membranes.

observed under fluorescent microscope. It should be pointed out that to prevent the fluorescent dye from diffusing into the films and the consequent "false-positive" phenomenon, the bacteria were centrifuged and washed thoroughly with fresh LB medium before the static adhesion tests.

The representative fluorescence microscopy images showing *E. coli* attachment to the coated/uncoated RO membranes are shown in Figure 8. On the bare RO membrane surface, significant bacterial adhesion and formation of a confluent biofilm of *E. coli* were observed at the end of the 1 h incubation. However, no such film formed on the zwitterion-coated RO membrane. It has further been shown by Cheng and co-workers[22] that after about 9-day flowing adhesion experiments, polysulfobetaine modified surface reduced more than 99% of the adhesion of bacteria compared to that on bare glass surfaces. In future work, rigorous testing will be performed to quantify this antifouling behavior.

The antifouling property of zwitterionic materials in inhibiting the formation of biofilm is attributed to the electrostatically induced strong hydration. The excellent ability of pSBMA to reduce protein adsorption as well as bacterial adhesion has been shown before. This work provides a technique for grafting a stable, defects-free thin layer of zwitterionic polymer onto delicate substrates, and rendering them the ultralow fouling properties for various applications.

CONCLUSIONS

Antifouling, surface-attached zwitterionic ultrathin (30 to 100 nm) films were synthesized using initiated chemical vapor deposition (iCVD) for the first time. The zwitterionic moiety in the iCVD film was confirmed by FTIR and XPS results. The content of zwitterionic units in the copolymer was controlled precisely in the iCVD process.

The motivation to use the iCVD synthesis process was demonstrated by depositing iCVD zwitterionic thin films on commercial RO membranes, where traditional solution-phase modifications were not favored because of the harsh conditions involved. The capabilities of the all-dry iCVD process in the surface modification of delicate substrates were demonstrated.

The iCVD zwitterionic coating on RO membrane is highly smooth as confirmed by AFM measurements. The coating thickness on an RO membrane was shown to be comparable to the film thickness on Si and can be controlled in situ. However, increasing the thickness of the coatings increases the surface roughness and decreases the permeation rates. For a 30 nm coating with the composition of 35% sulfobetaine, the permeation flux was reduced by ~15% compared to bare RO membranes. It is possible to further decrease the coating thickness and obtain higher flux. The coating left the salt rejection of the membrane intact. Furthermore, the cross-linker in the copolymer and the MA grafting improved the coating stability compared with non-grafting coatings. The enhancement in antifouling performance was exhibited by the static cell adhesion tests with *E. coli*. The attachment of bacteria is readily prevented by coating the membranes with iCVD zwitterionic thin film.

Combining the high stability and the significant antifouling performance, this surface-tethered antifouling zwitterionic thin film made the prolonged usage of RO membranes possible. Future work will investigate techniques to optimize membrane permeability and extensively characterize the antifouling performance of the membrane.

■ ASSOCIATED CONTENT

Supporting Information. Further details are given in Figures S1 and S2. This material is available free of charge via the Internet at http://pubs.acs.org.

■ AUTHOR INFORMATION

Corresponding Author
*E-mail: kkg@mit.edu.

■ ACKNOWLEDGMENT

The authors would like to thank the King Fahd University of Petroleum and Minerals in Dhahran, Saudi Arabia, for funding the research reported in this paper through the Center for Clean Water and Clean Energy at MIT and KFUPM. We thank Jonathan Shu from Cornell Center for Materials Research (CCMR) for his help with XPS measurements.

■ REFERENCES

(1) Shannon, M. A.; Bohn, P. W.; Elimelech, M.; Georgiadis, G. J.; Marinas, B. J.; Mayes, A. M. *Nature* **2008**, *452*, 301–310.
(2) Herzberg, M.; Elimelech, M. *J. Membr. Sci.* **2007**, *295*, 11–20.
(3) Lin, N. H.; Kim, M.; Lewis, G. T.; Cohen, Y. *J. Mater. Chem.* **2010**, *20*, 4642–4652.
(4) Griebe, T.; Flemming, H. C. *Desalination* **1998**, *118*, 153–156.
(5) Qin, J.-J.; Liberman, B.; Kekre, K. A. *Open Chem. Eng. J.* **2009**, *3*, 8–16.
(6) Wei, X.; Wang, Z.; Zhang, Z.; Wang, J.; Wang, S. *J. Membr. Sci.* **2010**, *351*, 222–233.
(7) Freger, V.; Gilron, J.; Belfer, S. *J. Membr. Sci.* **2002**, *209*, 283–292.
(8) Adout, A.; Kang, S.; Asatekin, S.; Mayes, A. M.; Elimelech., M. *Environ. Sci. Technol.* **2010**, *44*, 2406–2411.
(9) Sun, Q.; Su, Y.; Ma, X.; Wang, Y.; Jiang, Z. *J. Membr. Sci.* **2006**, *285*, 299–305.
(10) Kang, G.; Liu, M.; Lin, B.; Cao, Y.; Yuan, Q. *Polymer* **2007**, *48*, 1165–1170.
(11) Harris, J. M. *Poly(Ethylene Glycol) Chemistry: Biotechnical and Biomedical Applications*; Plenum Press: New York, 1992.
(12) Tu, S.-C.; Ravindran, V.; Den, W.; Pirbazari, M. *AIChE J.* **2001**, *47*, 1346–1362.
(13) Krishnan, S.; Weinman, C. J.; Ober, C. K. *J. Mater. Chem.* **2008**, *18*, 3405–3413.
(14) Chen, S.; Zheng, J.; Li, L.; Jiang, S. *J. Am. Chem. Soc.* **2005**, *127*, 14473–14478.
(15) Kitano, H.; Mori, T.; Takeuchi, Y.; Tada, S.; Gemmei-Ide, M.; Yokoyama, Y.; Tanaka, M. *Macromol. Biosci.* **2005**, *5*, 314–321.
(16) Futamura, K.; Matsuno, R.; Konno, T.; Takai, M.; Ishihara, K. *Langmuir* **2008**, *24*, 10340–10344.
(17) Jiang, S.; Cao, Z. *Adv. Mater.* **2010**, *22*, 920–932.
(18) Li, G.; Cheng, G.; Xue, H.; Chen, S.; Zhang, F.; Jiang, S. *Biomaterials* **2008**, *29*, 4592–4597.
(19) Zhang, Z.; Chen, S.; Chang, Y.; Jiang, S. *J. Phys. Chem. B* **2006**, *110*, 10799–10804.
(20) Chang, Y.; Liao, S.-C.; Higuchi, A.; Ruaan, R.-C.; Chu, C.-W.; Chen, W.-Y. *Langmuir* **2008**, *24*, 5453–5458.
(21) Ladd, J.; Zhang, Z.; Chen, S.; Hower, J. C.; Jiang, S. *Biomacromolecules* **2008**, *9*, 1357–1361.
(22) Cheng, G.; Li, G.; Xue, H.; Chen, S.; Bryers, J. D.; Jiang, S. *Biomaterials* **2009**, *30*, 5234–5240.
(23) Zhang, S. F.; Rolfe, P.; Wright, G.; Lian, W.; Milling, A. J.; Tanaka, S.; Ishihara, K. *Biomaterials* **1998**, *19*, 691–700.
(24) Chang, Y.; Chen, S.; Zhang, Z.; Jiang, S. *Langmuir* **2006**, *22*, 2222–2226.
(25) Rodriguez Emmenegger, C.; Brynda, E.; Riedel, T.; Sedlakova, Z.; Houska, M.; Bologna Alles, A. *Langmuir* **2009**, *25*, 6328–6333.
(26) Louie, J. S.; Pinnau, I.; Reinhard, M. *J. Membr. Sci.* **2011**, *367*, 249–255.
(27) Lee, H.; Lee, B., P.; Messersmith, P., B. *Nature* **2007**, *448*, 338–342.
(28) Baxamusa, S. H.; Im, S. G.; Gleason, K. K. *Phys. Chem. Chem. Phys.* **2009**, *11*, 5227–5240.
(29) Martin, T. P.; Kooi, S. E.; Chang, S. H.; Sedransk, K. L.; Gleason, K. K. *Biomaterials* **2007**, *28*, 909–915.
(30) Xu, J.; Gleason, K. K. *Chem. Mater.* **2010**, *22*, 1732–1738.
(31) Baxamusa, S. H.; Gleason, K. K. *Adv. Funct. Mater.* **2009**, *19*, 3489–3496.
(32) Tenhaeff, W. E.; Gleason, K. K. *Chem. Mater.* **2009**, *21*, 4323–4331.
(33) Tenhaeff, W. E.; Gleason, K. K. *Langmuir* **2007**, *23*, 6624–6630.
(34) Martin, T. P.; Lau, K. K. S.; Chan, K.; Mao, Y.; Gupta, M.; O'Shaughnessy, W. S.; Gleason, K. K. *Surf. Coat. Technol.* **2007**, *201*, 9400–9405.
(35) Martin, T. P.; Sedransk, K. L.; Chan, K.; Baxamusa, S. H.; Gleason, K. K. *Macromolecules* **2007**, *40*, 4586–4591.
(36) Ozaydin-Ince, G.; Gleason, K. K. *J. Vac. Sci. Technol., A* **2009**, *27*, 1135–1143.
(37) Lin- Vien, D.; Colthup, N. B.; Fateley, W. G.; Grasselli, J. G. *The Handbook of Infrared and Raman Characteristic Frequencies of Organic Molecules*; Academic Press: New York, 1991.
(38) Chan, K.; Gleason, K. K. *Langmuir* **2005**, *21*, 8930–8938.
(39) Spanos, C. G.; Badyal, J. P. S.; Goodwin, A. J.; Merlin, P. J. *Polymer* **2005**, *46*, 8908–8912.
(40) Ferlita, R. R.; Phipps, D.; Safarik, J.; Yeh, D. H. *Environ. Prog.* **2008**, *27*, 204–209.
(41) Ghayeni, S. B. S; Beatson, P. J.; Schneider, R. P.; Fane, A. G. *J. Membr. Sci.* **1998**, *138*, 29–42.
(42) Baxamusa, S. H.; Gleason, K. K. *Thin Solid Films* **2009**, *517*, 3536–3538.
(43) Lau, K. K. S.; Gleason, K. K. *Adv. Mater.* **2006**, *18*, 1972–1977.
(44) Rahardianto, A.; Shih, W.-Y.; Lee, R.-W.; Cohen, Y. *J. Membr. Sci.* **2006**, *279*, 655–668.
(45) Xu, P.; Drewes, J. E.; Kim, T.-U.; Bellona, C.; Amy, G. *J. Membr. Sci.* **2006**, *279*, 165–175.
(46) Into, M.; Jonsson, A.-S.; Lengden, G. *J. Membr. Sci.* **2003**, *242*, 21–25.

(47) Kim, S. H.; Kwak, S.-Y.; Sohn, B.; Park, T. H. *J. Membr. Sci.* **2003**, *211*, 157–165.
(48) Tan, K.; Obendorf, S. K. *J. Membr. Sci.* **2007**, *305*, 287–298.
(49) Holmlin, R. E.; Chen, X.; Chapman, R., G.; Takayama, S.; Whitesides, G., M. *Langmuir* **2001**, *17*, 2841–2850.
(50) Wang, H.; Chen, S.; Li, L.; Jiang, S. *Langmuir* **2005**, *21*, 2633–2636.